Journal of Ovonic Research Vol. 10, No. 3, May - June 2014, p. 89 - 100

GADOLINIUM DOPED ZnO NANOCRYSTALLINE POWDERS AND ITS PHOTOCATALYTIC PERFORMANCE FOR DEGRADATION OF METHYL BLUE UNDER SUNLIGHT

M.I. GHOURI, E. AHMED, N.R. KHALID, M. AHMAD, M. RAMZAN, A. SHAKOOR, N.A. NIAZ*
Department of Physics, Bahauddin Zakariya University, Multan 60800, Pakistan

This work reports the effect of gadolinium (Gd^{+3}) doping on the structural and physical properties of ZnO nanoparticles. Sol-gel method was utilized to synthesize ZnO and Gd-doped ZnO particles. ZnO powders were prepared from zinc acetate dehydrate and ethanol, using as precursor and solvent respectively. The synthesized powders were calcined at 300^{o}C for 1 hour. Structural, morphological properties and I-V characteristic of undoped ZnO and Gd-doped ZnO powders were investigated by XRD, SEM, FTIR and dc electrical measurements. The hexagonal wurtzite phase of the ZnO powders, without any secondary phase was revealed from the X-ray diffraction measurements. No significant change in the lattice parameters, as could be expected from Gd^{+3} incorporation, was observed. The crystallite size varies from 8.83 nm to 21.85 nm when Gd^{+3} concentrations vary from 0 wt% to 4 wt%. The photocatalytic activity of Gd-doped ZnO with different Gd loading was compared with undoped ZnO in the degradation of methyl blue (MB). It was observed that the rate of degradation of MB over Gd-doped ZnO increases with Gd loading up to 2 wt% and then decreases. The electrical properties of ZnO and Gd-doped ZnO powders were also investigated. The results showed the increase in current with Gd loading. Accordingly, resistivity was decreased with Gd loading.

(Received April 2, 2014; Accepted June 6, 2014)

Keywords: Photocatalytic degradation; Methyl blue; Gd-doped ZnO nanopowders; solgel;

1. Introduction

Zinc oxide (ZnO), an n-type wide band non-toxic compound semiconductor, with a direct band gap of 3.37 eV, coupled with its large exciton binding energy of 60 meV at room temperature. ZnO can be applied as photocatalysts, luminescence, surface acoustic wave filters, piezoelectric transducers, actuators, gas sensors, solar cells, window heating, varistors, UV lasers, FETs, pharmaceuticals and cosmetics, etc [1-3]. Zinc oxide (ZnO) is also an antibacterial biocompatible material and exhibits high mechanical, thermal and chemical stability. Due to its exceptional physical and chemical qualities, it can be used extensively in information technology, bio technology and environmental technology as next generation technologies [4-5]. At ambient temperature, ZnO has a non-centrosymmetric wurtzite crystal structure with polar surfaces [6].

For the degradation of toxic and non biodegradable compounds to carbon dioxide and inorganic constituents, semiconductors are being used as catalysts [7-8]. In this process, conduction-band electrons and valence-band holes would be generated on its surface. ZnO is a semiconductor and electron hole pair that is created upon irradiation with light having energy greater than its band gap energy, move to the surface of ZnO where they cause oxidation-reduction reaction with water and oxygen. Oxidizing reaction with H_2O produces hydroxyl radical and

* Corresponding author: niazpk80@gmail.com

reduction reaction with O_2 produce superoxide anion. When the cell membrane of bacteria is in contact with the powerful oxidants, it will be decomposed and consequently the bacteria will die. The body of the bacteria will eventually be decomposed into carbon dioxide and water. This process makes it suitable for wastewater purification at ambient temperature and atmospheric pressure [2].

ZnO has also been considered as a suitable alternative for TiO_2 due to its similar band and lower cost. Moreover, it exhibits better performance in the degradation of organic dye molecule in both acidic and basic media. The intrinsic defects of ZnO are beneficial to setting up catalytic systems, which are expected to degrade the environmental contaminants. It is well known that the properties of nanomaterials depend on their size, morphology, and dimensionality. Thereby, diverse morphologies of ZnO nanostructures have been synthesized for different applications. The decrease of the size of ZnO nanostructures is feasible to obtain more surface area and great efforts have been made to decrease the crystal size and enlarge the ratio of surface to volume. It is accepted that surface area and surface defects play an important role in photocatalytic activities of metal oxide, which could be attributed to the variation of the surface area, surface defects and band gap caused by the incorporation of dopant ions. It was reported that the surface conditions of ZnO were modified with the incorporation of dopant ions and its photocatalytic properties were greatly enhanced [1]. The synthesis of semiconductor nanoparticles via solution routes is advantageous in many ways as the growth, size and morphology can be controlled. Sol-gel method is very simple and does not require any special equipment. ZnO prepared by this method have well crystalline phase and small crystallite size, which benefit to thermal stability and photocatalytic activity.

In this study, we prepared gadolinium (Gd) doped ZnO nanoparticles by sol gel method with various Gd concentrations using gadolinium oxide (Gd_2O_3) as Gd source. Photocatalytic activity of the synthesized samples was evaluated via the degradation of methyl blue in aqueous solutions under sun light irradiation.

2. Experimental

The main materials used in this study were zinc acetate dehydrate [$Zn(CH_3CO_2).2H_2O$] and gadolinium oxide Gd_2O_3. ZnO and Gd-doped ZnO nanopowders were synthesized by sol gel process. Zinc acetate dehydrates and ethanol was used as a precursor material and the solvent, respectively. Zinc acetate dehydrate (5 gm) was dissolved in 100 ml of absolute ethanol and stirred with a magnetic stirrer at room temperature for half an hour, to be mixed thoroughly. Then 1M solution of NÅH was added under continuous stirring in order to get pH value of reactants between 8 and 11. The white powder was obtained after stirring this solution at 80^0C for 6h and drying it at 100^0C in an oven for 12h. For doped ZnO nanoparticles the appropriate amounts of Gd_2O_3 were dissolved in nitric acid (HNO_3) which was added in the homogenized and clear solution of Zinc acetate dehydrate and ethanol. The remaining procedures were the same as described above. The powder was calcined for 1 hour in a furnace at 300^oC. The calcined powders were finally pulverized with a mortar and pestle.

Powder X-ray diffraction (XRD was used for crystal phase identification and estimation of the particle size. The X-ray diffraction (XRD) measurements were carried out by using Shimadzu X-ray diffractometre equipped with CuKα radiation (λ=1.5406Å). A Fourier transform infrared spectrophotometer (FTIR) Perkin-Elmer System 2000 was used to determine the specific functional groups. The morphology of the samples was inspected with scanning electron microscopy (SEM) JEOL Japan, JSM-5910). IV characteristics and electrical resistivity measurements were made by two probe method. For this purpose dc power supply and sensitive electrometer model 2400 (Kiethley) were used.

A basic aniline dye, MB was used as a probe molecule to evaluate the photocatalytic activities of the Gd^{+3} ions doped ZnO nanocrystallites. In each experiment, a 0.1g amount of photocatalyst was added into beaker (Pyrex glass containing 100 ml of methyl blue solution with an initial concentration of 0.02mg/100ml water. Prior to solar irradiation, each suspension was magnetically stirred in the dark for 30 min to established adsorption-desorption equilibrium. Then the solution was exposed to sunlight along with stirring. Experimental place was Multan (30^0 15/

N, 71^0 36/) during the month (September 15-30, 2010). At irradiation time of every 30min, the concentration of the methyl blue was monitored using a UV- vis spectrophotometer (Hitachi U-2001) by checking the absorbance at 510 nm. The degradation rate of methyl blue was calculated based on the following formula:

$$\text{Degradation (\%)} = [(C_0 - C)/C] \times 100$$

Where C_0 is the initial concentration of MB mgL^{-1} and C is the concentration at each interval of time in mgL^{-1}.

3. Results and discussion

X-ray diffraction analysis is made to determine the crystallite size and structure of the synthesized samples. Fig. 1 shows the diffraction patterns of ZnO powders synthesized by the sol-gel method calcined at 300°C and with loading of different atomic fractions of Gd^{+3} ions. Only the peaks corresponding to wurtzite ZnO were observed, JCPDS File No. 05-0664 [9]. The absence of other isolated phases may suggest the possible incorporation of Gd^{+3} within the host ZnO lattice. The XRD pattern of all the Gd doped ZnO catalysts are almost similar to that of ZnO, suggesting that there is no change in the crystal structure upon Gd doping. However, considering that the ionic radii of Gd^{+3} (0.94Å) is much larger than that for Zn^{+2} (0.74 Å), the exchange between Gd^{+3} and Zn^{+2} species should have been reflected by a strong distortion of the ZnO unit cell and hence, of the corresponding lattice parameters. Although the lattice parameter values exhibited a random variation with the nominal Gd^{+3} contents, no appreciable effect on "c" and "a" parameters was observed when compared to undoped ZnO [10]. Fig. 1 shows the XRD pattern of the ZnO, synthesized in the basic alkaline medium. It is observed that the sample is highly crystalline as evident from the XRD pattern in which broad peaks with high intensity extended over the 2θ scale. The peak observed at $2\theta = 31.85^0$, 34.49^0, 36.3^0, 47.45, 56.71^0, 62.77^0, 67.89^0 corresponds to the lattice planes (100), (002), (101), (102), (110), (103) and (112) respectively, indicative of wurtzite hexagonal structure of ZnO [9]. The lattice constants for hexagonal ZnO powders are reported in JCPDS data, a = 3.24982Å and c = 5.20661Å. The lattice constant corresponding to the main peak of ZnO at $2\theta = 36.3^0$ are obtained by the following equation,

$$\frac{1}{d^2_{(hkl)}} = \frac{4}{3}\left(\frac{h^2 + hk + k^2}{a^2}\right) + \frac{l^2}{c^2}$$

The lattice constant calculated by using above equation are "a = 3.2438Å" and "c = 5.2054 Å". The lattice constants are in good agreement with standard data. The crystallite size was estimated using the full width at half maximum (FWHM) of high intensity peak (101) appear at $2\theta = 36.3^0$ using the Scherer equation

$$D = k\lambda/\beta cos\theta$$

Where D is the crystallite size in nm, k = 0.89 which is a constant, λ is the wavelength of X-ray radiation in nm, θ is the Bragg angle in radians and β is the FWHM in radians. The crystallite size of ZnO nanopowder was found to be 14.81 nm. Fig. 1 also shows XRD patterns of Gd-doped ZnO nanopowder with different gadolinium contents. The XRD patterns of Gd-doped ZnO are almost similar to that of undoped ZnO, suggesting that there is no change in crystal structure. However, it should be noted that Gd-doped samples have a wider and lower intense diffraction peaks. Moreover, the XRD peaks of Gd-doped ZnO continuously get broader with increase in the Gd loading. The crystallite size of Gd-doped ZnO calculated by Scherrer equation is smaller when compared with that of undoped ZnO, which decreases with the increase in Gd loading as shown in Table 1. The decrease in the crystallite size of Gd-doped ZnO is mainly attributed to the formation of Gd−O−Zn on the surface of the doped samples [10], which hinders the growth of crystal grains. The XRD patterns of 3 wt% and 4 wt% Gd-doped ZnO nanopowders

are almost similar to that of undoped ZnO. However, it should be noted that the 3 wt% and 4 wt% Gd-doped samples have a sharp and large intense diffraction peaks than 0.5, 1 and 2 wt% Gd-doped ZnO. It is noted that the crystallite size of 3 wt% and 4 wt% Gd-doped ZnO is larger when compared with that of 0.5, 1 and 2 wt% Gd-doped ZnO which shows that the solubility limit of gadolinium ions in ZnO crystal lattice is close to 2 wt% and the excess gadolinium ions may precipitate out on the particle surfaces [10-11].

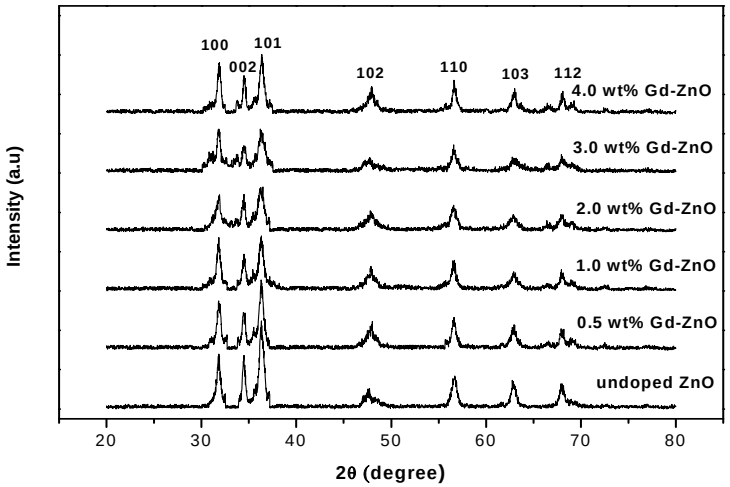

Fig. 1 XRD pattern of undoped and Gd doped ZnO nanopowders calcined at 300^{0}C for 1hour.

Fig. 2 shows XRD patterns of 3 wt% Gd-doped ZnO nanopowders synthesized at different temperatures. All XRD patterns in the figure are similar to that of undoped ZnO. No remarkable variation on lattice parameters of host ZnO was observed. Further it is observed that the crystallite size, calculated from Scherer formula, increases with increasing temperature from 100^{0}C to 300^{0}C as shown in Table 2, which means that crystallinity has been improved. The sharpening of peaks can be understood by considering the merging process induced by thermal treatment. Sharpening is a consequence of crystal growth, due to intergrain diffusion [12-13].

Table 1 Physical characteristics of undoped ZnO and Gd-doped ZnO photocatalysts calcined at 300^{0}C.

Samples	**Crystallite size from XRD (nm)**	**Lattice Parameter (Å)**		**c/a**	**Unit cell volume (nm)**
		a	c		
Undoped ZnO	14.81	3.2438	5.2054	1.6047	0.04743
0.5 wt% Gd- ZnO	14.32	3.2502	5.1826	1.5945	0.04741
1 wt% Gd-ZnO	11.06	3.246	5.1935	1.6000	0.04739
2 wt% Gd-ZnO	8.83	3.2502	5.0768	1.562	0.04644
3 wt% Gd-ZnO	15.89	3.248	5.1579	1.5886	0.04712
4 wt% Gd-ZnO	21.85	3.2502	5.2321	1.6098	0.04787

Table 2 The effect of calcinations temperature and time on crystallite size of different samples.

Samples	Calcination Conditions		Crystallite size (nm)
	Temperature ^{o}C	Time (hour)	
3 wt% Gd-ZnO	100	1	11.06
3 wt% Gd-ZnO	200	1	14.81
3 wt% Gd-ZnO	300	1	15.89
3 wt% Gd-ZnO	200	1	14.81
3 wt% Gd-ZnO	200	1.5	11.06
3 wt% Gd-ZnO	200	2	8.83

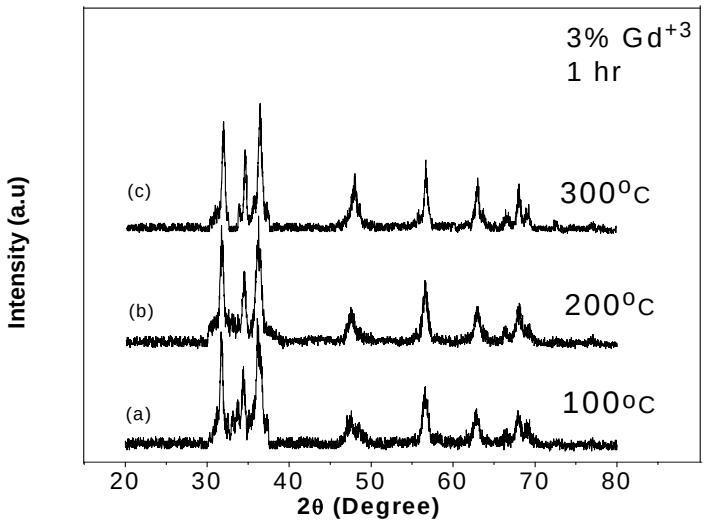

Fig. 2 XRD patterns of 3 wt% Gd-doped ZnO nanopowders calcined at (a) 100^{o}C (b) 200^{o}C (c) 300^{o}C.

Fig. 3 shows XRD pattern 3 wt% Gd-doped ZnO nanopowders calcined at 200^{0}C for different times. All XRD patterns exhibit wurtzite structure. No remarkable variation is observed in lattice parameters. Moreover, the XRD peaks get broader and less intense with increase in calcinations time from 1h to 2h [14].

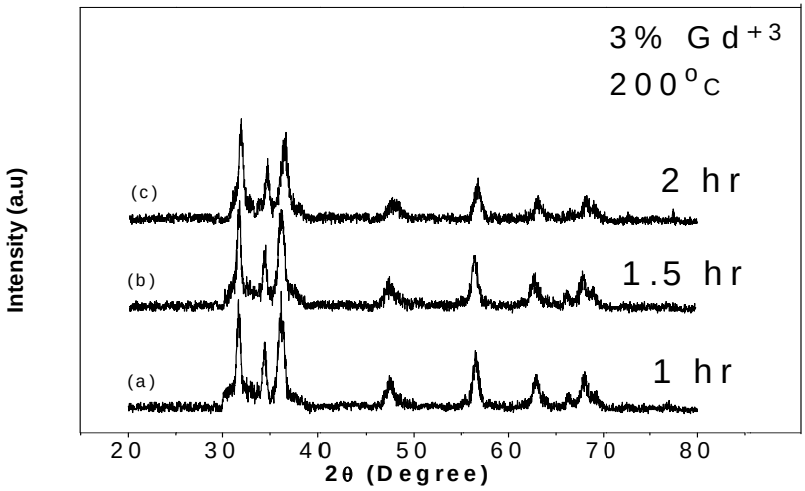

Fig. 3 XRD patterns of 3 wt% Gd-doped ZnO nanopowders calcined at 200°C for different times.

Figs. 4-5 displays the SEM images of surface morphology of undoped and Gd-doped ZnO nanocrystalline powders calcined at 300^0C. Both images show closely packed nearly spherical and randomly oriented grains. The tendency of high agglomeration among smaller crystallites was noted with dopant of gadulinium. We observed that undoped ZnO nanocrystalline powder consists of larger grains. The agglomeration of particles was decreased with doping of gadolinium.

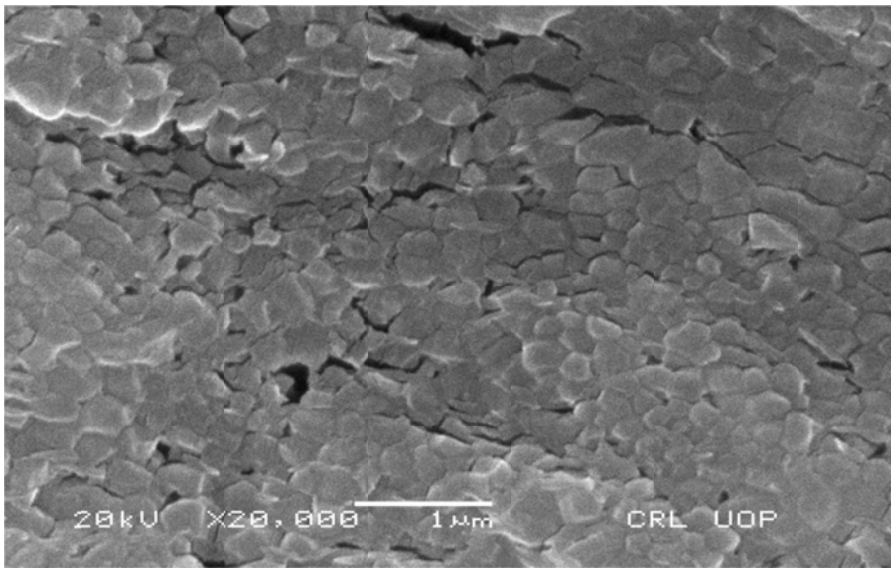

Fig. 4 SEM image of undoped ZnO powders.

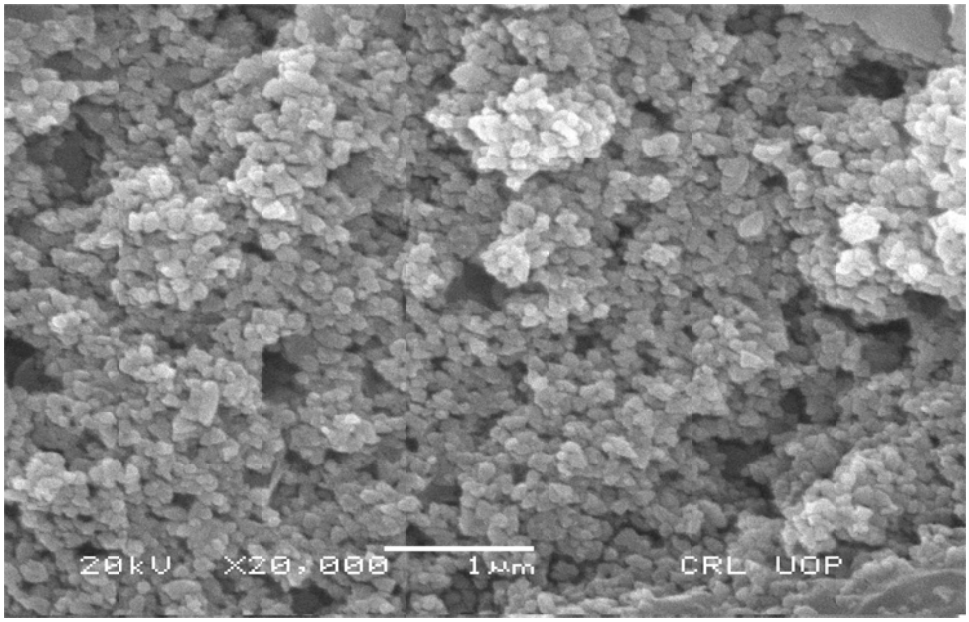

Fig. 5 SEM image of 3 wt% Gd-doped ZnO powders.

FTIR spectra of undoped ZnO and Gd-ZnO samples in the region 4000-400cm^{-1} are shown in Fig. 6-7. The main absorption band due to O-H stretching of hydroxyl group is observed at 3455 cm^{-1}. The bands at 2850 and 2925 cm^{-1} correspond to C-H (acetate) stretching. The absorption peaks at 2244 and 2354 cm^{-1} correspond to the existence of CO_2 molecules in air. Two principal absorption peaks are observed at 1420 cm^{-1} and 1560 cm^{-1}, corresponding to the asymmetric and symmetric C=O stretching of zinc acetate. The peak at 1560 cm^{-1} indicates the formation of ZnO [15]. The weak shoulder band at 1340 cm^{-1} could be ascribed to nitrate symmetric stretching mode. The deformation bands of C=O can also be observed at 1020 cm^{-1}. The band at 645 cm^{-1} corresponds to O-H bending of hydroxyl group. The absorption band at 525 cm^{-1} corresponds to Zn-O stretching of ZnO [16-18].

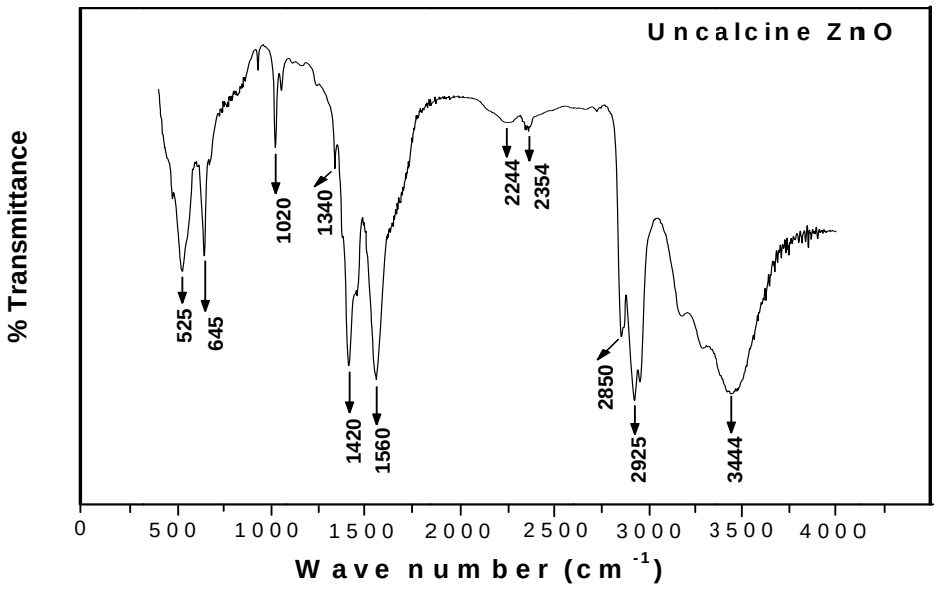

Fig. 6 FTIR spectra of uncalcined ZnO particles.

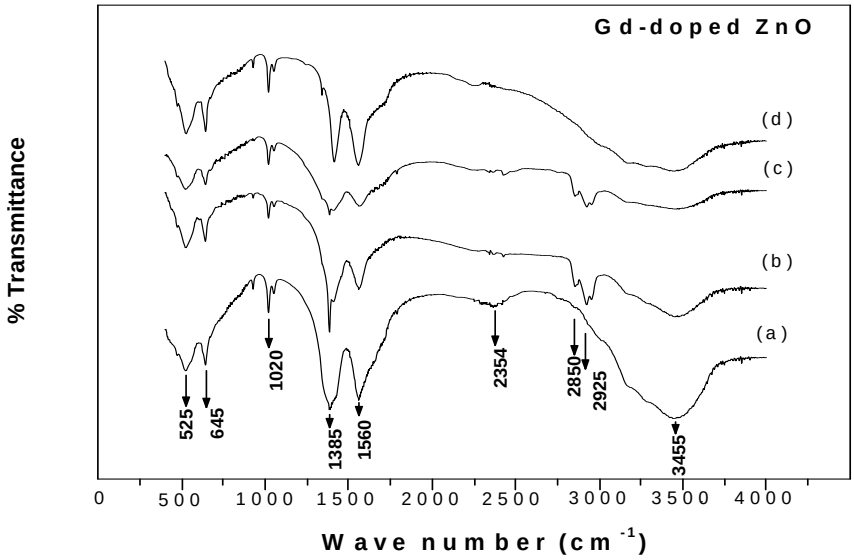

Fig. 7 FTIR spectra of (a) 1 wt% Gd-ZnO (b) 2 wt% Gd-ZnO (c) 3 wt% Gd-ZnO (d) 4 wt% Gd-ZnO powders.

Fig.8 shows the degradation of MB over undoped ZnO and Gd-doped ZnO with different gadolinium doping. It is clearly seen that rate of photocatalytic degradation of Gd-doped ZnO catalyst is much higher when compared with that of undoped ZnO. It is interesting to note that the degradation rate of the catalyst increases with increase in the Gd^{+3} loading up to 2 wt% and then decreases. Thus, it is concluded that the optimum loading of Gd^{+3} is 2 wt%, which may be more efficient for separating photo induced electron-hole pairs and enhance the photocatalytic activity because of small particle size. The photocatalytic activity of Gd-doped ZnO is due to the formation of Zn−O−Gd bond formed on the surface of ZnO [10]. The reason for the high activity of 2 wt% Gd-doped ZnO and the effect of Gd loading on the photocatalytic activity can be explained by the following mechanism. Under the irradiation of Gd-doped ZnO nanoparticles, Gd^{+3} works as an electron scavenger, this may react with the superoxide species and prevent the holes-electrons recombination, and thus increases photodegradation efficiency. With the increase in Gd^{+3} concentrations, the surface barrier becomes higher, the space charge region becomes narrower, and hence the electron-hole pairs are efficiently separated by the large electric field. On the other hand, the photocatalytic activity of 3 wt%, and 4 wt% Gd^{+3} loaded ZnO is even lesser than undoped ZnO due to the screening effect with the increase in the concentration of Gd^{+3} ions, the penetration depth of light into ZnO can greatly exceed the space charge layer. Therefore, the recombination of photo generated electron-hole pairs becomes easier, which led to a lower photocatalytic activity of ZnO for MB degradation [19-20]. Hence, 2 wt% is the optimum amount of Gd^{+3} needs for good photocatalytic activity.

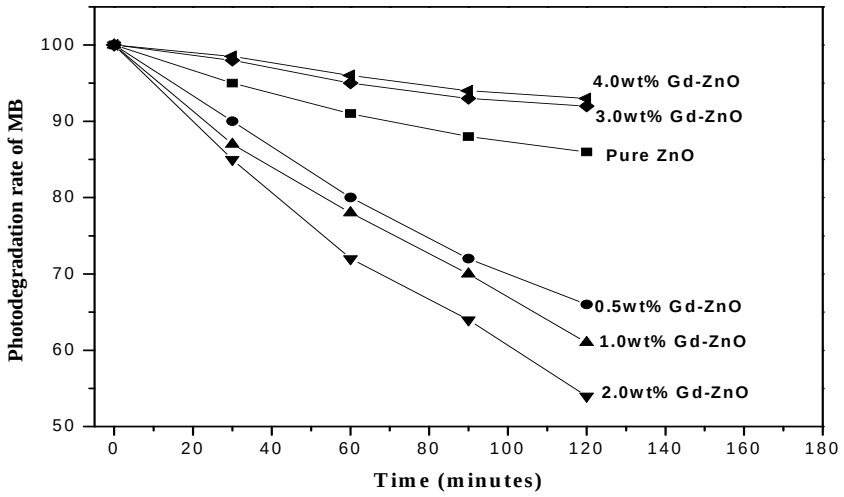

Fig. 8 Methyl blue degradation under sunlight (initial concentration of MB = 20mg/L, and catalyst = 1g/L, pH =9).

A plot of the current (*I*) as a function of the applied voltage (*V*) for undoped and Gd-doped ZnO nanopowder at room temperature is shown in Fig. 9. The curves have a slope of approximately unity at 15 Volt, implying that the conduction is ohmic at this voltage. It was seen that all the samples exhibit n-type conductivity. It is well known that n-type conductivity in undoped ZnO is due to the oxygen vacancy and interstitial zinc atom, which act as donors [21]. At a specific voltage the current increases with an increase in gadolinium concentration.

The electrical resistivity, of a material depends on it free-carrier concentration (n), and its carrier mobility (μ). The effects of doping gadolinium concentration and calcination temperatures on the electrical resistivity of the doped and undoped ZnO nanoparticles are presented in Fig. 10. The electrical resistivity of the doped ZnO nanoparticles is lower than that of the undoped ZnO nanoparticles. It is seen that as gadolinium is added to the starting solution, the electrical resistivity decreases with the increase in loading. A lower resistivity value was obtained at 4 wt% Gd-doped ZnO. An initial decrease in the resistivity is due to an increase in the free-electron concentration with gadolinium incorporation in the ZnO nanoparticles. In other words, it can be attributed to the optimal incorporation of gadolinium atoms into the lattice, increasing the donor concentration and contributing to a decrease of the resistivity [17]. Afterwards, the increase observed in the electrical resistivity with the subsequent addition of gadolinium to the starting solution could be also attributed to the reduction in the grain size which reduces the majority carrier mobility because of increasing the scattering process. The adding more gadolinium in the starting solution will increase the gadolinium concentration in the nanopowder, then the high gadolinium concentration will also increase the scattering process and therefore the majority carrier mobility is decreased.

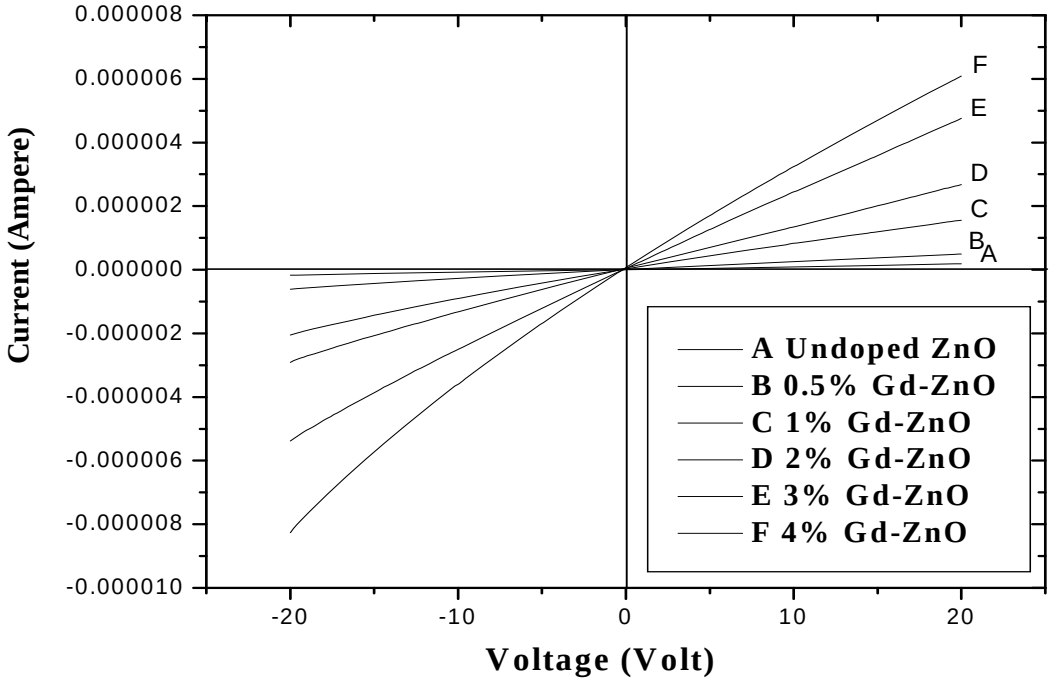

Fig. 9 The IV characteristics of doped and undoped ZnO at room temperature.

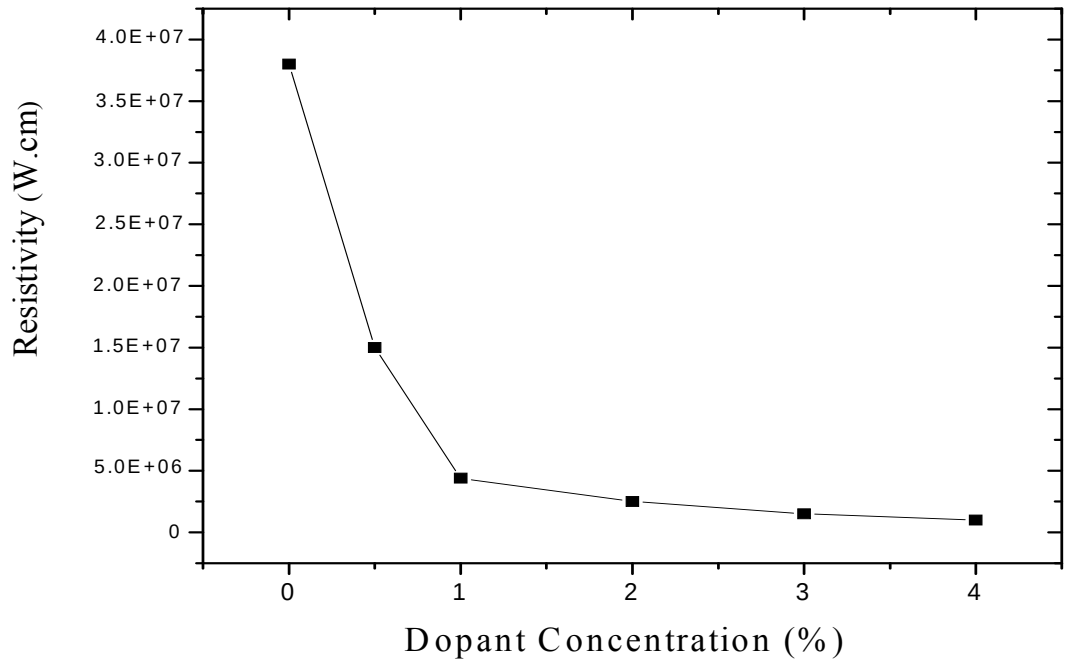

Fig. 10 The effect of gadolinium loading on the electrical resistivity of the doped and undoped ZnO nanopowder.

4. Conclusion

ZnO nanocrystalline powders doped with up to 4 wt% gadolinium (Gd^{+3}) have been prepared. These powders have been indexed as wurtzite structure with the smallest average crystallite size of about 14.46 nm and grain size (from SEM) of 76 nm. The Gd doping significantly affects the particle size, the particle size of Gd-doped ZnO is much smaller when compared with that of undoped ZnO. The FTIR analysis confirms the formation of ZnO. The photoactivity of undoped and doped ZnO nanocrystalline powders have been evaluated by monitoring the photo-bleaching of the aqueous solutions of methyl blue (MB) dye under sunlight. The photocatalytic activity of the 3 wt% Gd-doped ZnO is higher than those of undoped ZnO. This reduction is important for ZnO nanoparticles to be used as UV shielding agents to protect organic substrates. The I-V curves show that all the samples exhibit ohmic conduction mechanism. The gadolinium incorporation affects the resistivity of ZnO nanocrystalline powders. The 4 wt% Gd-doped ZnO nanocrystalline powder have a lower resistivity than the other nanocryatalline powders. It is observed that calcination improve the crystallinity of the samples.

Acknowledgement

All the authors would like to thank the Higher Education Commission, Pakistan for financially supporting this project.

References

[1] T. Jia, W. Wang, F. Long, Z. Fu, H. Wang, Q. Zhang, Journal of Alloys and Compounds, **484**, 410 (2009)
[2] K. C. HsiÅ, S. C. LiÅ, Y. J. Chin, Material Scienceand Engineering A, **447**, 71 (2007)
[3] V. R. Shinde, T. P. Gujar, C. D. Lokhande, R. S. Mane, S. H. Han, , Materials Chemistry and Physics, **96,** 326 (2006)
[4] A. Mclaren, T. V. Solis, G. Li, S. C. Tsang, Journal of American Chemical Society, **131**, 12540 (2009)
[5] Y. J. Kwon, K. H. Kim, C. S. Lim and K. B. Shim, J. Ceramic Processing Research, **3**,146 (2002).
[6] U. Ozgur, Y. I. Alivov, C. Liu, A. Teke and M. A. Reshchikov, Journal of Applied Physics, **98,** 41301, (2005)
[7] L. C. Chen, Y. J. Tu, Y. S. Wang, R. S. Kan, C. M. Huang, J. Photochemistry and Photobiology A: Chemistry, **199,** 170 (2008).
[8] R. Ullah, J. Dutta, J. Hazardous Materials, **156**, 194 (2008)
[9] Joint Committee on Powder Diffraction Standards (JCPDS) File No. 05-0664.
[10] Y.Zhou, S.X.Lu, and W.G.Xu, Wiley Interscience. DOI 10.1002/ep.10318 (2008).
[11] T. Tsuzuki, Z. Smith, A. Parker, R. He, X. Wang, Journal of the Australian Ceramic Society, **45**, 58 (2009)
[12] G. T. Delgado, C. I. Z. Romero, S.A M. Hernandez, Solar Energy Materials & Solar cells, **93,** 55 (2009)
[13] M. Mohammadi, M. R. Rokn-Abadi and H. Arabshahi, Indian Journal of Science and Technology, **3,** 2, (2010)
[14] A. Abdel Aal, Sawsan A. Mahmoud, Ahmad K. Aboul-Gheit, Materials science and Engineering C, **29,** 831 (2009).
[15] R. Ullah, J. Dutta, IEEE-ICET (2006).
[16] T. Sahoo, M. Kim, M. H. Lee, L. W. Jang, J. W. Jeon, J. S. Kwak, I. Ko, I. Lee, Journal of alloys and compounds, **491**, 308 (2010).
[17] M. Sahal, B. Hartiti, A. Ridah, M. Mollar, B. Mari, Microelectronics Journal, **39**, 1425 (2008).

[18] S. Senthilkumaar, K. Rajendran, S. Banerjee, T.K. Chini, V. Sengodan, Materials Science in Semiconductor Processing, **11,** 6 (2008)
[19] P. Pawinrat, O. Mekasuwandumrong, J. Panpranot, Catalysis Communications, 10, 1380 (2009).
[20] Q. XiÅ, J. Zhang, C. XiÅ, X. Tan, Materials Science and Engineering B, **142**, 121 (2007)
[21] Y. Caglar, M. Zor, M. Caglar, S. Ilican, Journal of optoelectronics and advanced materials, **8,** 1867 (2006).